ISSN 2522-9400 **European Modern Studies Journal** *Vol 8 No 1*
available at www.journal-ems.com

DOI: 10.59573/emsj.8(1).2024.29

Analysis of Three-Dimensional Modeling and Simulation of Boiler Shell and Tube Heat Exchanger Baffles

Kannie Winston Kuttin [1,2], Alexander Yaw Osei [3,4]*
[1]Institute of Clean Coal Technology, East China University of Science and Technology, Shanghai 200237, China
[2]Engineering Research Centre of Resource Utilization of Carbon-containing Waste with Carbon Neutrality, Ministry of Education, China
[3]Kumasi Technical Institute, Industrial Mechanics Department, Kumasi, Ghana
[4]Akenten Appiah Menka University of Skill Training and Entrepreneurial Development, Kumasi, Ghana

Abstract. The goal of this research is to model a three-dimensional steam-producing plant heat exchanger for industrial operations. With a certain tube bundle structure, inlet temperatures and the velocity of the tube and shell sides are used as input factors in the current investigation. The heat transfer study takes hot flue gas inside the tubes and steam on the shell side into account. The model was designed and simulated using ANSYS 2020 fluent for the analysis, which was authenticated by contrasting the output results to actual in-house operating data. According to the computational results, the proposed design allowed for a 9°C rise in shell-side fluid temperature. It has been discovered that installing more baffles in the steam flow channel increases the fluid pressure moving through the heat-exchanger. When compared to the WKX110 model, the velocity along the PMX110 length was more uniform. The velocity distribution indicates that the velocity is particularly high at the baffle turns. This is helpful because the high velocity encourages high convection transfer of heat in the region; therefore, the installation of this baffle improves heat exchange efficacy. The numerical PMX110 and WKX110 findings were validated with experimental data and found to be in good agreement.

Key Words: Boiler heat exchanger, Baffles, Tube-side, Shell-side, Numerical Simulation

Introduction

Boilers are being used for a variety of applications, including fuel changes, energy generation, and new inventions in fields such as materials and water chemistry, among others. As market rivalry develops, boilers have been designed nearer to the limit, requiring more understanding of dynamical behaviour. Due to strict regulation of global manufacturing, increased emphasis is placed on boiler safety, energy efficiency, and dynamic performance. Many components serve as a base of support for the boiler in order for it to satisfy its set steam or heat needs. There are tubes bundles that convey flue gas, water and/or steam all through the system; equipment are preserved from flying percolate and ash by the soot blowers; burners; exiting flue gas is recover by the economizer to pre-heat inlet water to further process to steam; heat exchangers, and many other systems that help the steam-producing boiler be energy efficient. In the boiler system, heat is transferred between two streams via boiler heat exchangers. In order to integrate energy and reduce the need for external heat sources, the exchange might occur between two process streams or between a utility stream and a process stream (Khayal, 2018). A heat exchanger can be categorized as fired or unfired depending on how it utilized the two process streams. Several research have focused on exchanger accessories and operational characteristics of heat exchangers. Gomaa et al. (2016) investigated

* Corresponding Author

the three-way concentric-tube heat-exchanger both experimentally and numerically, focusing on double tubular heat-exchanger. (Bougriou & Baadache, 2010) investigated a novel form of heat-exchanger, shell and tube duo centric heat exchangers. García-Valladares (2004) produced a thorough transient state one-dimensional computational model of the fluid-dynamic and thermal behaviour of threefold concentric tube heat-exchangers. Costa and Queiroz (2008) reported on design optimization of shell-and-tube heat exchanger. The specified issue involved discrete variables and the minimization of the heating surface area. Dubey et al. (2014) offer a detailed thermal examination of the impact of severe loading circumstances on heat-exchanger performance. Pandita et al. (2023) performed research that forecasted the performance of a heat exchanger in their study. Using various inclinations of baffle angles, the efficiency of the heat-exchanger was studied. Samal (2013) uses ANSYS software tools to model a shell and tube heat-exchanger with 7 tubes and a shell diameter of 90 mm with a helical baffle and investigate the temperature and flow pattern inside the shell. Raj and Ganne (2012) evaluated the effects of varying baffles angle inclination on properties of transfer of heat and flow of fluid of a shell-and-tube heat-exchanger for three distinct baffle angles in their study. Computational fluid dynamics (CFD) models are becoming increasingly prevalent in the energy processes, which is subject to the influence of various mass transfer, heat transfer, chemical kinetics and reaction rates. CFD models can reduce the time and money required to design an energy reactor and its accessories and determine the output of these complex process based on particular parameters by employing the appropriate modeling techniques. A model is similar and straightforward system than the system it portrays. A model's objective is to allow the analyst to forecast the effect of variations to the system in order to decrease the likelihood of failure, prevent resources over or under utilization, eliminate unpredicted problems, and optimize systems efficiency. Many commercial boiler heat-exchangers with less baffles made of steel have been designed for use in steam boiler plants. However, the tubes stretch, droop, and vibrate due to a few baffles that are not proportional to the size of the boilers. Based on the aforementioned issue, this research aims to investigate existing industrial boiler heat exchanger designs by modelling and simulating a three-dimensional heat exchanger in a steam-generating boiler for industrial operations powered by biomass. The primary goal of this study is to study the configurational effect of baffles on exchanger efficiency and analyze performance of the heat exchanger with hot fluid in the form of exhaust gas from the boiler and cooling fluid in the form of water taking into account temperature profiles, velocity, and pressure drops.

Experimental Setup and Materials

The Luigi PMX110 model at Log & Lumber Limited was studied for 6 hours on three consecutive days to acquire data for future modelling of the 2-baffle and 5-baffle heat exchangers with the goal of investigating two-baffle heat exchangers. The PMX110 Prime boiler superheater heat exchanger (2-baffles) and all of its elements were manufactured of 306L stainless steel. The PMX110 heat-exchanger has parallel 13 stainless-steel tubes bundle with an inner diameter of 105mm. Decarbonated water was used as the shell-side fluid in this experiment. The transfer of heat inside the shell and the tubes was measured in order to correctly model the PMX110 heat-exchanger and utilize the data for the modelling of the five baffles (WKX110) design. Boundary conditions temperature on the exterior wall were maintained constant and monitored to aid in the construction of the theoretical and numerical models. The boiler was operated continuously for two hours before the data were measured to ensure a consistent temperature of the heat exchanger. Using a 5W cumulative step, the rates of heat transfer of 5-95W range were examined. The rate of flow of steam was held constant at 14/30 and was measured in a given volume of steam on an hourly basis using a flash recovery flask. The four independent J-type thermocouple modules were used to record the steady state temperatures of the steam to evaluate thermal performances of the PMX110 heat-exchanger.

Four thermocouples were fitted on the cold section’s outlet and inlet, and four on the tube section's outlet and inlet. Three rotameters were used to measure the fluid flow rates. The incoming fluid temperature remained constant by using a thermostatic flow tank. To decrease heat loss to the environment, the entire system was lagged with rubber insulation. To measure the local pressure and temperature, pressure gauges and two resistance detectors for temperature (MF1200) were mounted on each intake and exit of the PMX110. Before the trials, the providers calibrated the temperature detectors and pressure gauges. The allowable pressure and temperature indicator slipups were pegged at 0.1 kPa and 0.1 °C, respectively. To gather data, all thermal indicator sensors were linked through a digital display device. The thermohydraulic parameters of the PMX110 were tested and analysed in this experiment under the counter flow situation. In this work, we focus on the effect of baffles on the thermohydraulic properties of the PMX110. Data is gathered until the system achieves a stable condition. Each step is repeated three times to ensure repeatability.

Numerical Model

The heat exchanger models were modelled with ANSYS Workbench DesignModeler, and numerical simulations were run with Computational Fluid Dynamics (CFD) programs in the ANSYS fluent version 2020R1 software. The two most essential elements influencing the design of boiler heat exchanger systems are temperature and pressure (Nsofor et al., 2007). Many additional elements, such as start-up, shutdown, upset, dry-out, external loading supports, earthquake load, wind loading, pulsing pressure, and so on, have a substantial impact on heat exchanger functioning. Based on this data, the heat exchanger design datasheet was created in accordance with Tubular Exchanger Manufacturers Association (TEMA) requirements. Because heat exchanger process design is an open-ended problem, there were more variables constraints than restrictions. As a result, some of those factors might be adjusted to provide an efficient heat-exchanger and cost-effective design. Certain parameters of the process, such as the process flow rate, intake temperature, design and operating pressure values, maximum permitted pressure drop, and so on, were static, acting as calculation inputs as well as simulation fixed input constraints.

Mathematical Model

The motion of the working fluid in the exchanger system is described using the governing equations of momentum, energy, and mass continuity.

Energy Equation of fluid Model

The energy of volume of fluid is represented by equation (1):

$$\frac{\partial}{\partial t}(\rho E)+\nabla\cdot(\rho E V)=\nabla\cdot(k\nabla T)+\nabla\cdot(pV)+S_E \tag{1}$$

The energy source term S_E is used to determine heat transfer during evaporation and condensation.

The T, which is temperature, is treated as a variable for mass averaged in the VOF.

Thermal conductivity *k* is derived as (Kuzmin & Hämäläinen, 2014):

$$k=\alpha_l k_l+(1+\alpha_l)kv \tag{2}$$

The energy E is likewise treated as a variable for mass-averaged in the VOF is also calculated by:

$$E=\frac{\alpha_l\rho_l E_l+\alpha_v\rho_v E_v}{\alpha_l\rho_l+\alpha_v\rho_v} \tag{3}$$

where E_v and E_l are dependent on the phase's specific heat C_v and temperature, as determined by caloric equation (Fadhl et al., 2015):

$$E_l = c_{v,l}(T - T_{sat}) \tag{4}$$

$$E_v = c_{v,v}(T - T_{sat}) \tag{5}$$

Equation for Volume Fraction (Continuity)

The continuity equation has the following form when the physical principle of mass conservation is applied to the fluid:

$$\nabla \cdot (\rho V) = -\frac{\partial \rho}{\partial t} \tag{6}$$

where V the velocity vector, ρ denotes density and t the time.

Thus, the VOF model's continuity equation for the secondary phase is represented by (7) (Kuzmin & Hämäläinen, 2014):

$$\nabla \cdot (\alpha_l \rho_l V) = -\frac{\partial}{\partial t}(\alpha_l \rho_l) + S_m \tag{7}$$

Transfer mass during condensation and evaporation is computed by the mass source term S_m. (Kuzmin & Hämäläinen, 2014):

Momentum Equation

Pressure, Gravitational, friction, and surface tension forces are assumed to be at work in the fluid. The continuous surface force *(CSF)* model is considered to take care of the influence of surface tension (Brackbill et al., 1992).

$$F_{CSF} = 2\sigma \frac{\alpha_l \rho_l C_v \nabla \alpha_v + \alpha_v \rho_v C_l \nabla \alpha_l}{\rho_l + \rho_v} \tag{8}$$

While the coefficient of surface tension is denoted by σ and C represent surface curvature.

Taking into consideration the forces stated above, the momentum equation of the VOF is as follows (Fadhl et al., 2015):

$$\frac{\partial}{\partial t}(\rho V) + \nabla \cdot (\rho V V^T) = \rho g - \nabla p + \nabla \cdot \left[\mu(\nabla V + (\nabla V)^T - \frac{2}{3}\mu(\nabla \cdot V) I \right] + F_{CSF} \tag{9}$$

where g = acceleration due to gravity,
p = pressure
I = unit tensor
μ = dynamic viscosity

Reynolds Number of Tube-Side

The observed mixing action is the criteria for differentiating between laminar and turbulent flow.

$$\mathrm{Re}_t = \frac{\rho_t u_t \pi d_t}{\mu_t} \tag{10}$$

where μ_t denotes the viscosity of the tube-side fluid,
u_t denotes velocity of fluid within the tubes,
ρ_t denotes density of fluid within the tubes.

Nusselt Number

Prandtl number *(Pr* and Reynolds number *(Re)* are functions of Nusselt number *(Nu)*. The following Petukhov-Kirillov equation was used for turbulent flow.

$$Nu_t = \frac{(f/2)\mathrm{Re}_t \mathrm{Pr}_t}{1.07 + 12.7(f/2)^{1/2}(\mathrm{Pr}_t^{2/3} - 1)} \tag{11}$$

where friction factor f is determined by:

$$f = (1.58 \ln \mathrm{Re}_t - 3.28)^{-2} \tag{12}$$

Coefficient of Heat Transfer

The tube-side coefficient of heat transfer is stated as follows:

$$h_t = Nu_t \frac{k_t}{d_t} \tag{13}$$

where,

Nu_t is the Nusselt number for the tube-side fluid

k_t is the tube-side fluid thermal conductivity

d is inner diameter of tube

Tube-sheet Mean Metal Temperature

Un-tubed portion of tube-sheet:

$$T_{TS} = \frac{T_T - T_S}{2} \tag{14}$$

Tubed tube-sheet portion:

$$T_{TS} = T_T + (T_S - T_T)\frac{(\eta - F)}{(A/a)\left(1+\eta\frac{h_T}{h_S}\right)} \tag{15}$$

where,

T_T= Temperature of the fluid in the tube

T_S= Temperature of the fluid shell-side

h_T= coefficient of heat transfer of the tube-side

h_S = coefficient of heat transfer of the shell-side

$$\eta = \frac{A}{aK}\left[\frac{1+\frac{A}{aK}\tanh(K)}{\frac{A}{aK}+\tanh(K)}\right] \tag{16}$$

$$K = \sqrt{\frac{AhTL}{a12k}} \deg$$

where k = thermal conductivity of tube-sheet metal W/(m^{0}K)

L denotes the thickness of the tube-sheet in meters

$$F = \frac{1}{\cosh(K) + \frac{aK}{A}\sinh(K)} \tag{17}$$

in the case of a square pitch

$A = \pi dL$

$a = p^2 - \pi d^2/4$

d = tube ID, meters

P = tube pitch, meters

Tube-Side Hydraulic Analysis

The pressure reduction experienced by the fluid as it flows in the heat exchanger computed as by:

$$\Delta P_t = \left(4 f_t \frac{LN_p}{d_t} + 4N_p\right)\rho_t u_t^2 \tag{18}$$

where L is the length, of the tube

N_p is the number of passes

ρ_t is the density of the fluid moving inside the tubes

Total Coefficient Heat Transfer

U_c denotes the total coefficient of heat transfer for a clean surface.

$$\frac{1}{U_c} = \frac{1}{h_o} + \frac{1}{h_i}\frac{1}{d_i} + \frac{r_o \ln(r_o / r_i)}{k} \tag{19}$$

where h_o is the coefficient for shell-side heat transfer
h_i is the coefficient for tube-side heat transfer
r_o is the tube outer radius
r_i is the tube inner radius
k is the thermal conductivity materials

Geometrical Modeling and Meshing

3D simulations were performed to explore the CFD modelling of the effect of the five baffles against the two baffles heat exchanger. The ANSYS meshing (Figures 1 a and b) was used to discretize the heat exchanger design model into smaller nodes and elements through which a set of equations were solved. To a larger extent, the correctness of each solved model is closely connected to the meshing utilized. Initially, the domain was divided into coarse cells, and the temperature, velocity, and pressure were studied once the simulation had reached its conclusion. Although the study of Jouhara et al. (2016) demonstrates that the behavior of 2D and 3D geometries is the same, because of the relevance of velocity streamlines, 3D geometry was chosen for simulation. A mesh sensitivity analysis was performed to help with mesh selection. Because the quality of the meshing has a major impact on the simulation outcomes. Very fine, fine, coarse, and very coarse meshing techniques were used and compared: the size of the polyhedral elements was reduced from 2 mm to 1.2 mm for each mesh. The meshing sensitivity test revealed that the temperature difference between the very fine mesh and the fine mesh after 60 seconds was less than 0.5-degree lower. However, while choosing a mesh, the precision of the results of the simulation must be balanced against the computational time. Calculation time is very crucial for transient multi-phase simulation and might be a genuine difficulty.

(a)
(b)

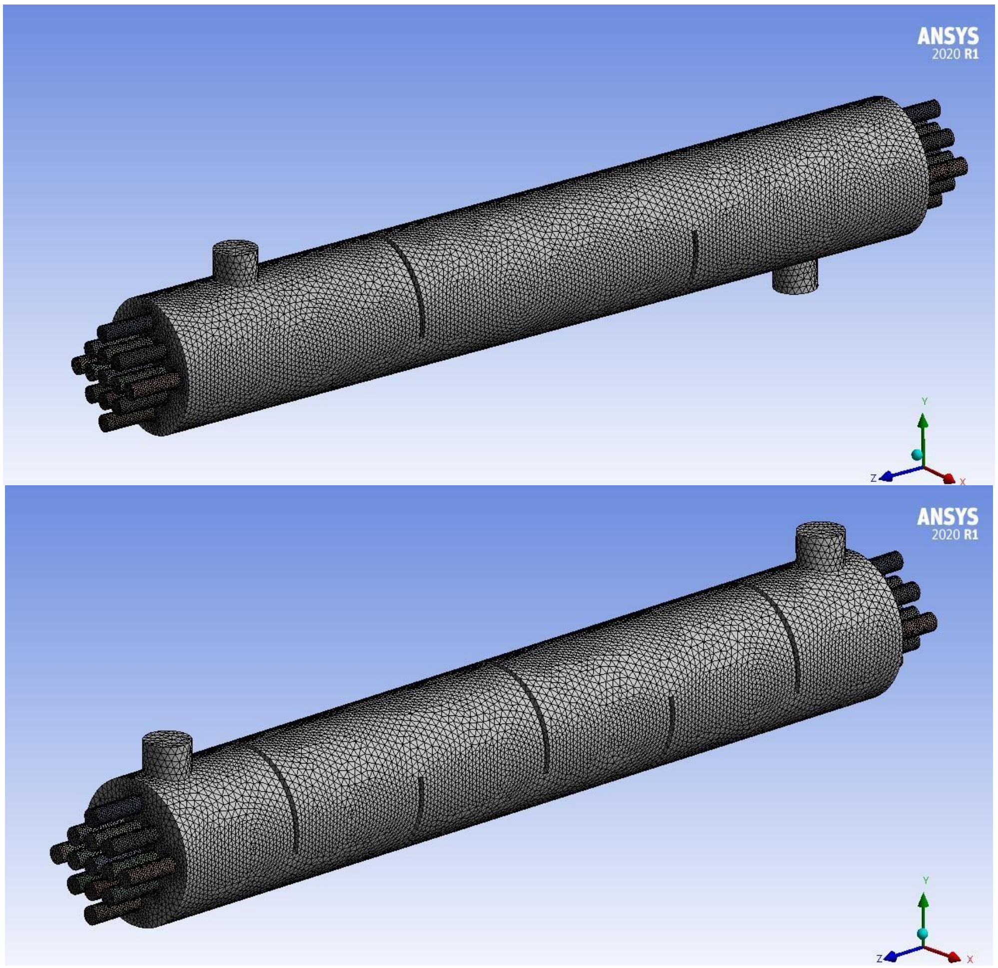

Figure 1. 3D mesh (a) PMX110 and (b) WKX110 heat exchangers

Boundary Conditions and Calculation Procedure

The working temperatures for both first phase and second phase were 120 and 527 degrees Celsius, respectively. The velocity for phase one and phase two were 0.4 and 0.5 m/s, respectively. $V_{tube} = 0.4\ ms^{-1}$ was assigned to the inner surface of the tubes, tube end sections. $V_{shell}=0.5\ ms^{-1}$ was also assigned to the inner surfaces of the shell, the outer surfaces of the tubes and tube-sheet and the baffles. The initial pressure for both phases is considered to be zero, therefore assigning $P_{shell/tube} = 0$ MPa, to the heat-exchanger's outputs on both the flue phase and steam phase. The inner walls of the flue pipes were subjected to a non-slip boundary condition. The second phase of the system was defined as adiabatic preventing any temperature loss due to lagging of the system elements with a zero-heat flux. The water and flue pipes were established as coupled wall boundary to facilitate heat transmission between the fluid zones and outer surface of the tubes.

To describe the dynamic behavior of the heat exchanger a transient two-phase flow, simulation was performed. To automatically alter the time step depending on the largest Courant-Friedrichs-Lewy figure at the boundary of the two phases, an adjustable time stepping approach was applied. In the model, a blend of the SIMPLE technique to couple pressure-velocity and a first-order upwind technique for energy and momentum determination is used. The model additionally employs geometry discretization and PRESTO for the interpolation schemes of volume fraction and pressure, respectively.

The primary phase of the system was designated as the working fluid (flue phase), while the secondary phase was categorized as the steam phase. The VOF approach was used in the modelling by including the necessary source terms into the flow controlling equations. The source terms, which govern transfer of heat and mass between the flue and vapor phases, have been coupled to FLUENT's major hydrodynamic equations.

Table 1. Boiler input data

Parameter	Variable	Unit
Temperature - tube-side	527	^{0}C
Velocity - tube-side	0.4	m/s
Pressure - tube-side	0	MPa
Temperature - shell-side	30	^{0}C
Velocity - shell-side	0.5	m/s
Pressure shell-side	0	MPa
Wall heat transfer coefficient	0.05	W/m^{2}K
Ambient temperature	25	^{0}C

Results and Discussion

Thermal-Hydraulic Analysis

Figures 2–5 depict the temperature, pressure, velocity, and velocity streamlines distribution contours of PMX110 and WKX110, respectively.

Table 2: Validation of the model Simulations and the experimental test

Model name	Temperature	Pressure	Velocity
Numerical PMX110	106.9°C	30.08 Pa	0.5610m/s
WKX110	117.8°C	41.11 Pa	0.492m/s
Experimental test	102.5°C	38.90Pa	0.610m/s

Temperature Threshold

Figure 2 shows temperature distribution of both PMX110 and WKX110. The outlet temperature of the WKX110 showed a high performance of 390.764°K (117.764 ^{0}C) as compared to the PMX110 result of 379.9°K (106.9°C). The locus of the infinite set of streamlines in the WKX110, vividly rooted at the opening point along the continuous originating segment confirms flow delay thereby indicting the rise in temperature. The shell side outlet temperature is determined to be consistent with the in-house operating data, with a deviation of less than 6%. Because there was vacant room for displacement margin owing to the flow direction, high-temperature zones were considered on the parallel planes of the baffles of both chambers of the heat-exchanges. The configuration, however, did not take into account the vacant areas at the corners in front of the heat-exchange baffles. Because of the vacant area, the simulation findings from the in-house operational data and the CFD study might have differed. Lowering the temperature disparity between flue gas and inlet water has the same impact in both scenarios, lowering aridity and increasing heat transfer by producing a greater temperature divergence between inlet water and flue gas. This is due to the inlet water absorbing the most heat from flue gas at temperature of 527°C before exiting the heat exchanger because of the counterflow nature of both streams. The findings also reveal that the proposed model (WKX110) and experiment data correspond well, with a maximum variation of 4.01% in terms of steam generation.

(a)

(b)

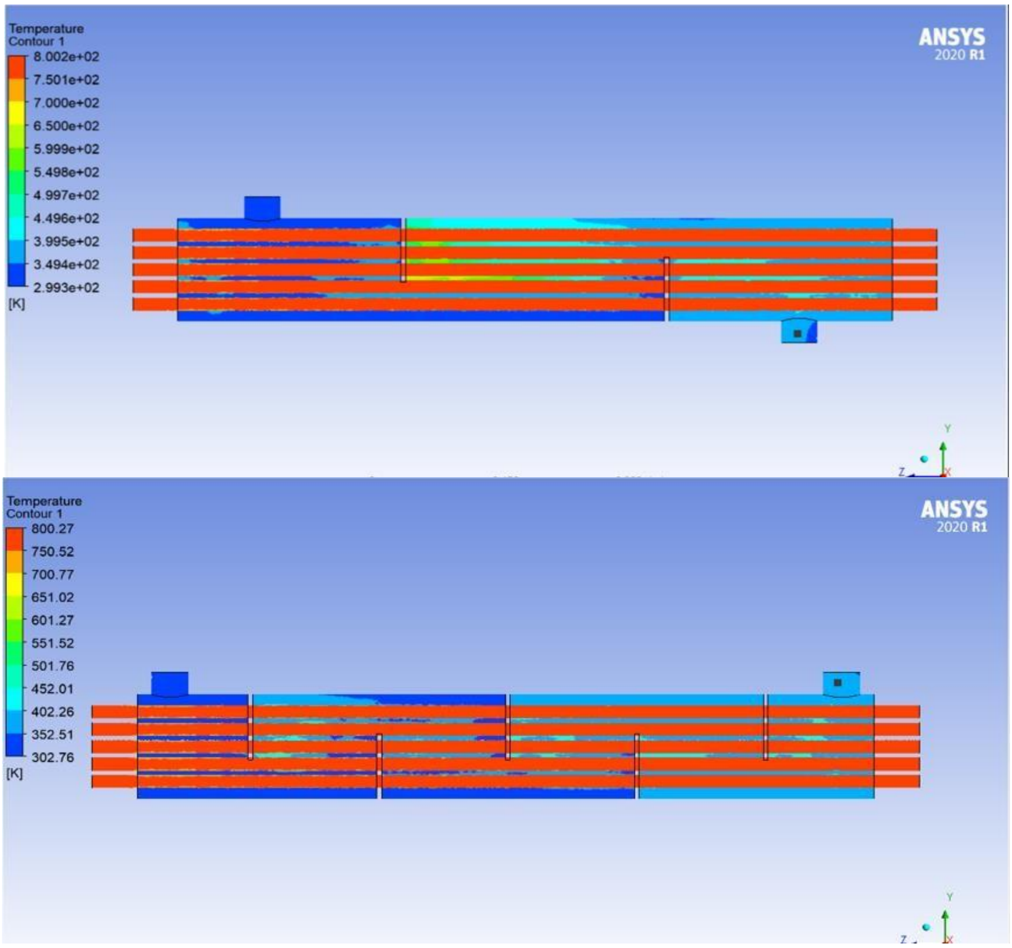

Figure 2. Temperature contours (a) PMX110 and (b) WKX110

Reduction in intake water temperature does not only result in a greater temperature difference between the flue gas and steam stream, but it also causes the commencement of heating of inlet fluid in the shell-side to occur sooner due to hot flue gas wall temperatures. The relation of intake water flow rate to flue gas flow rate had a substantial influence as well. Increased ratios resulted in faster heat transfer and concentration rates. The ratio increases from 0.6 to 1.2 result in 0.21 increase in steam generation efficiency. Lowering the flow rate ratio permits the shell-side water to remain at a lower temperature throughout the heat exchanger's length. As a result, the tube temperature is substantially lower than greater ratios of flow rate, increasing heat transmission.

Since condensation of vapor occurs rapidly at low temperature wall, the latent thermal load rises sharply as the incoming fluid temperature drops. The functional load increases somewhat as the temperature variance between the tube-side and shell-side also increases, especially in shell and tube heat exchangers (STHE). In contrast to the impact of tube-side fluid humidity, which shows that as relative humidity increases, the functional load falls and the latent load increases, as indicated in (Huzayyin et al., 2007) and (Liang et al., 1999).

Pressure Threshold

The pressure distribution shown in Figure 3 shows that the pressure steadily falls from the intake to the exit due to pressure drop caused by high turbulent flow or friction caused by the baffle. Significant pressure variations are observed in the steam stream due to the density of water, which is significantly higher than that of flue gas stream and the rise in pressure of fluid caused by the incidence of several baffles. The system self-generated pressure of the PMX110 outflow path was calculated as 30.0801 Pa compared to 41.1148 Pa for WKX110 which is higher than the design constraint. It is revealed that the number of baffles and configuration in the flow path of stream also increase the fluid pressure flowing through the heat-exchanger. The presence of the multiple flow impeding inserts, resulted in an increase in pressure and also has a varying effect on the net power output. Comparing the pressure difference between the two designs, there is clear 11.0347 Pa in favour of WKX110 indicating the consequence of having multiple baffles on the heat exchanger. Due to the compact nature of baffle spacing, increasing the number of baffles increases the pressure and coefficient of heat transfer on the shell-side while decreasing the value of correction factor. In the same vein pressure rises faster as the number of baffles increases. The pressure readings collected during experimental observations are compared to the predicted pressure estimated at static circumstances in Table 2. At lowest stream circumstances, the empty segment is 0.5, and the rotundity stream factor is 0.65. According to the streamline contours in figure 5, recirculation adjacent to the baffles increases turbulence eddies, which in turn increase pressure for the WKX110 model, whereas re-circulations are much less for the PMX110 model, which shows the resultant pressure. There is less pressure in the PMX110 than in the other model owing to smoother flow direction. From the Pressure distribution, it can be seen that the pressure gradually decreases from the inlet to the outlet; this is due to the pressure drop either due to friction with the wall or turbulent flow due to the baffle. Significant pressure changes are seen in the water fluid, this is due to the density of water which is much higher than air, and to the decrease in air pressure due to the presence of a lot of baffles.

(a)

(b)

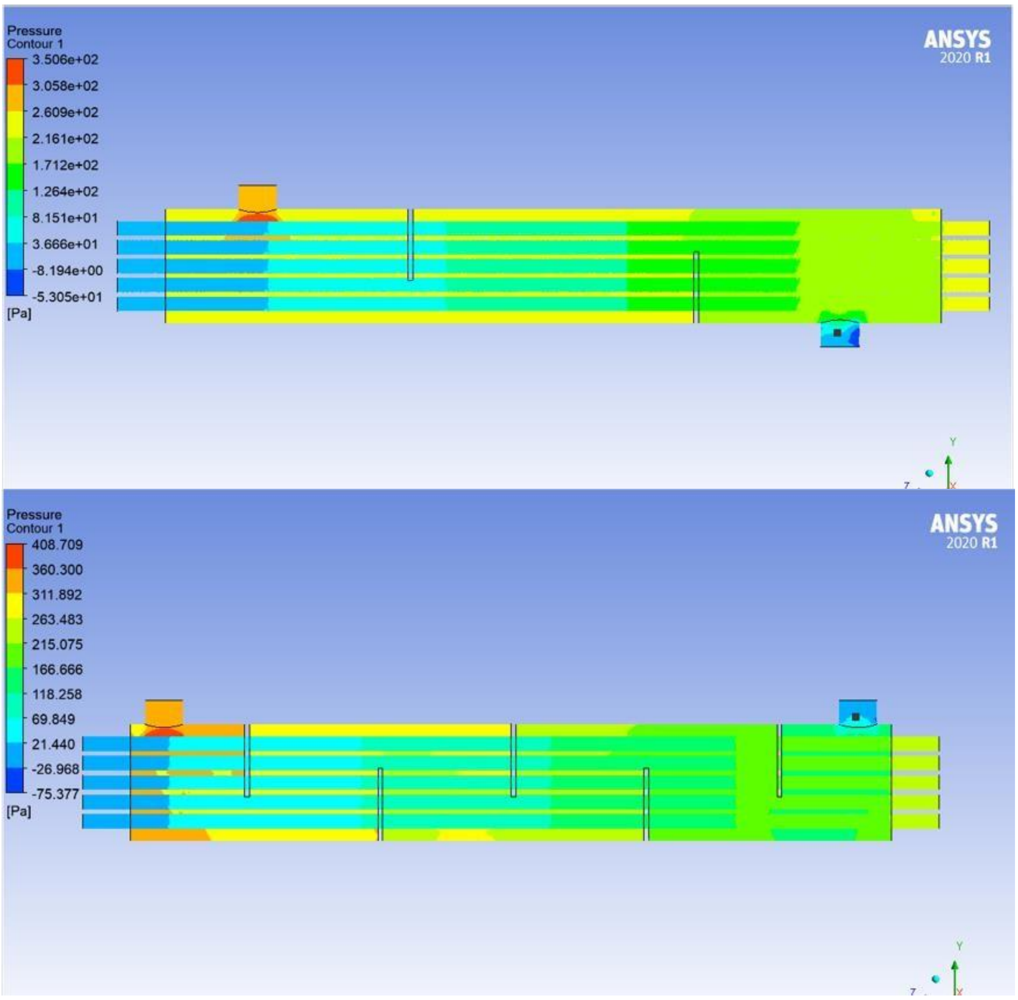

Figure 3. Pressure contours (a) PMX110 (b) WKX110

Velocity threshold

Figures 4 and 5 show the greatest streamlines of 3.188 and 2.911 for PMX110 and WKX110, respectively, indicating a velocity reduction for the PMX110 and a small rise in pressure for the PMX110. It was observed that increasing velocity increases flow rate of fluid, which lowers transfer heat but increases pressure drop. Figure 4 depicts the proposed model's prediction of average velocity drop. However, both models have a narrower range of velocity values throughout time. The PMX110 model forecasts the mean velocity drop value better.

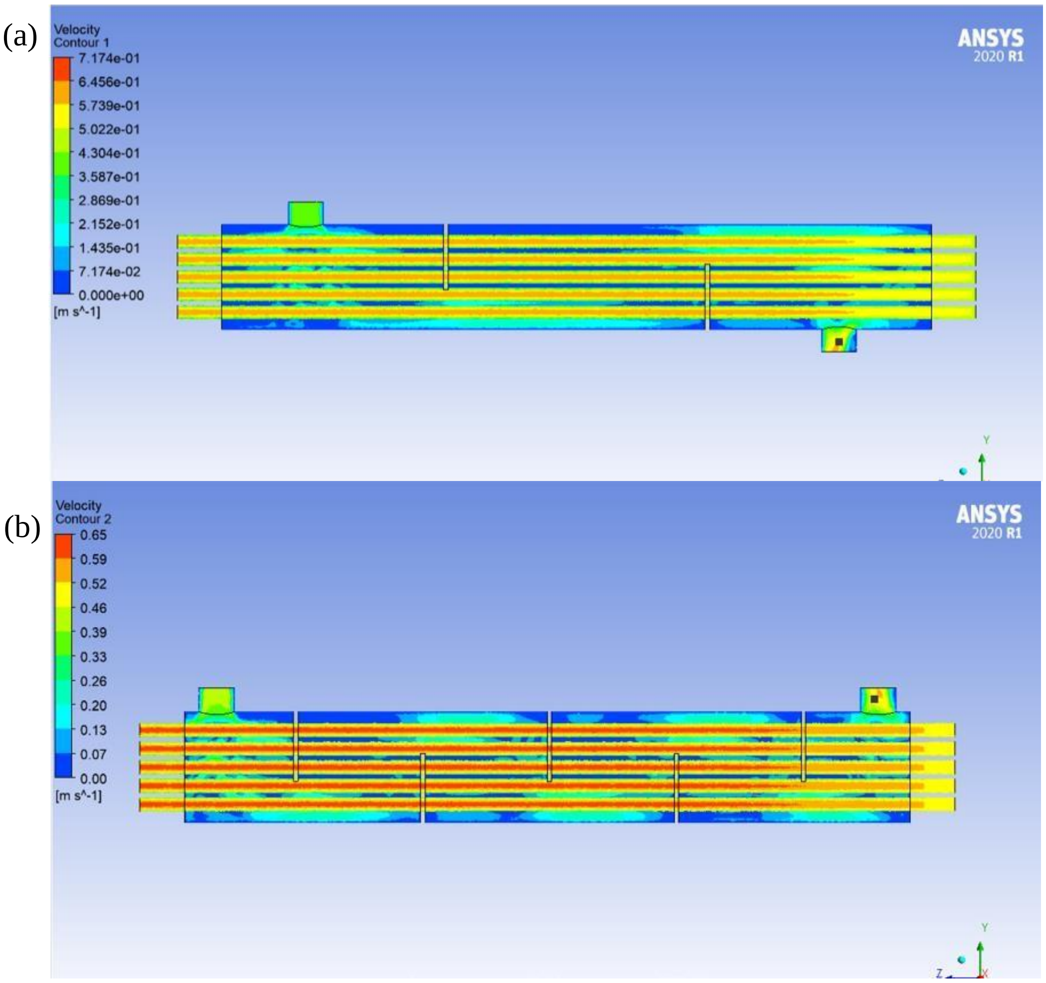

Figure 4. Velocity contours (a) PMX110 and (b) WKX110

Figure 5 shows that the velocity over the length of the PMX110 model is more uniform than that of the WKX110 model. The velocity contours show that velocity at baffle turns is significantly higher. it is not helpful because the high fluid flow velocity reduces heat transfer convection in the region at a high temperature, therefore the installation of this baffle improves heat exchange efficacy. Figure 5 shows the fluid flow velocity streamlines of both designs, with high velocity before each baffle. This comparatively low velocity value will make the heat-exchanger prone to fouling issues. These variables emphasize the significance of including additional limits, in addition to the core constraints of highest pressure drop and nominal surface area of heat transfer, to ensure the proposed exchanger's broad practicality. Because these restrictions are implemented in both designs, they do not exhibit the aforementioned shortcomings. At the outlet of the cold side, the highest velocity for PMX110 model is roughly 6 ms^{-1}, and there was a drastic reduction of velocity magnitude in the surfaces of the baffles up to zero. Comparing the two models, PMX110 offered an even fluid flow than WKX110.

(a)
(b)

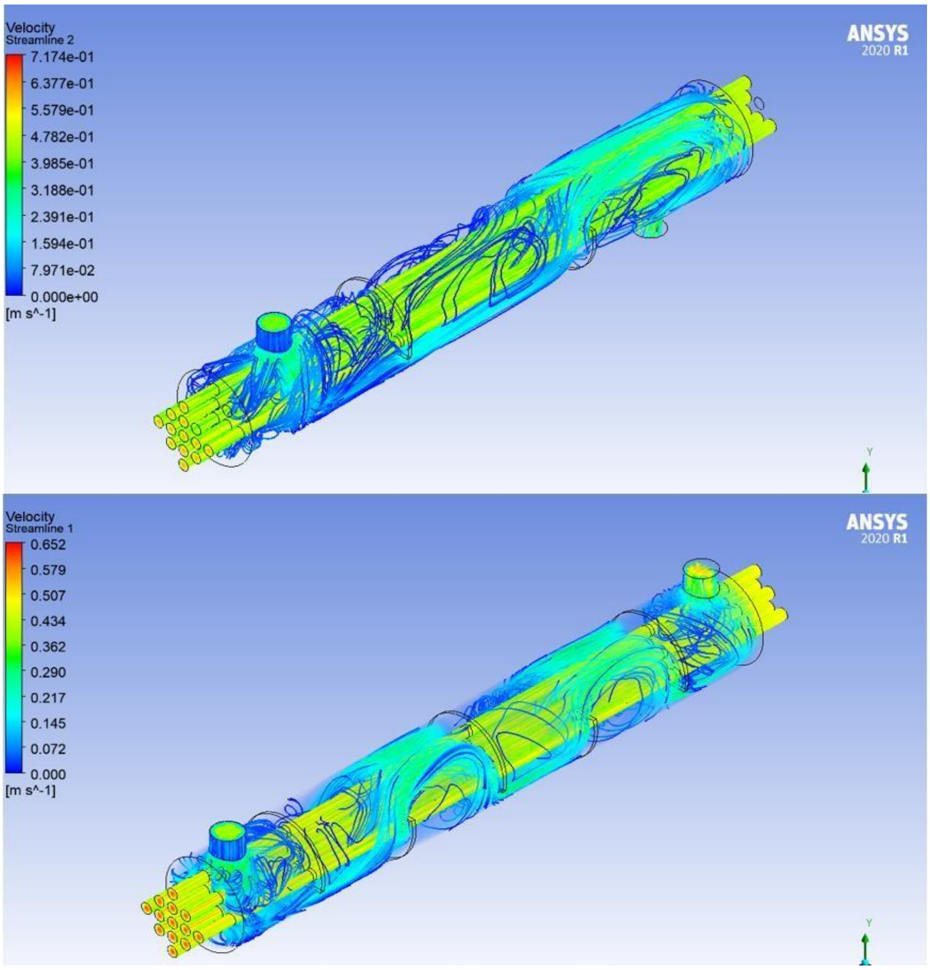

Figure 5. Velocity streamlines (a) PMX110 and (b) WKX110

Turbulence Variance Analysis

The imposed pressure drops of the heat-exchanger are determined by several parameters, the majority of which are interrelated to the geometrical features and installation of the heat-exchanger, namely tubes geometrical arrangement of the heat exchanger, overall configuration of the tubesheet and baffles. Aside from that, pressure is influenced by flow parameters such as the flow type and turbulent strength of the heat-exchanger.

Drag Effect

The Reynolds number is proportional to the coefficient of pressure drop and the amount of turbulence in the shell-side flow about the tubes of the heat exchanger. Regarding the variance set measurements, the observations for the pressure drop behavior were different for both designs. According to Figure 6, the coefficient of drag reduces as the Reynolds number increases. The intensity of the turbulence is proportional to the drag exerted by the heat-exchanger. The rise in turbulence from 2.5 to 5.2 reduces pressure fall by an average of 5.12%, respectively. Furthermore, increasing the intensity of turbulence up to 3.2% has a minor impact on the pressure. Similar findings may be made about the PMX110 and WKX110 models.

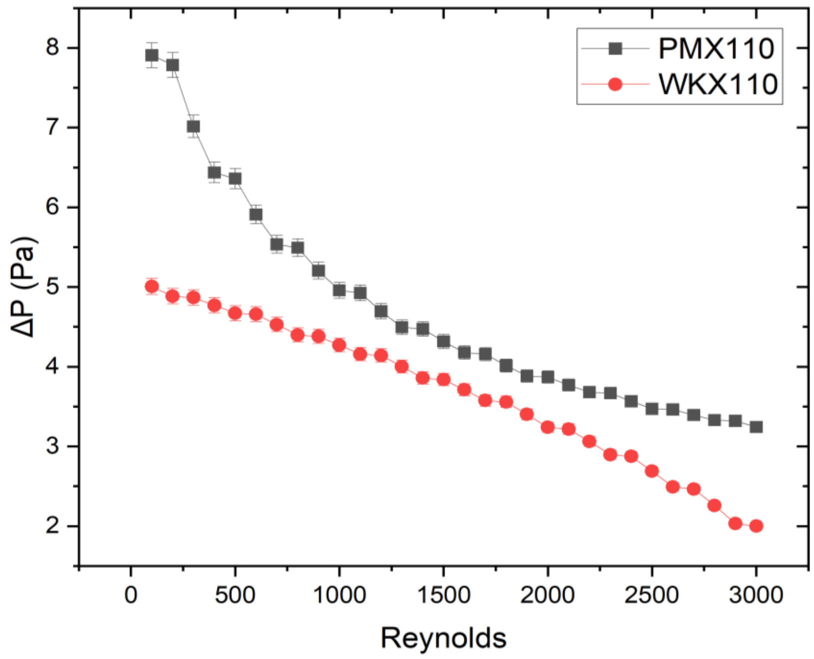

Figure 6. Drag and Reynolds number variance set

Change in Temperature -Reynolds Number Measurements

In terms of Reynolds number and quantities of heat transfer, an increase in Nusselt number increases the rate of the turbulence intensity, resulting in an increase in heat transfer thermal effectiveness and overall enhancement in the heat-exchanger. Maa, 20 and Tang, 2014 addressed the influence of turbulence strength on heat-exchanger efficacy by using the dimensionless number St^3/δ_{total} as a criterion for understanding heat-exchange improvement. Change in T rises as intensity of turbulence also rises, as indicated in Figure 7. This finding reveals that increasing the intensity of turbulence has a favorable influence on the total efficacy of the heat-exchanger.

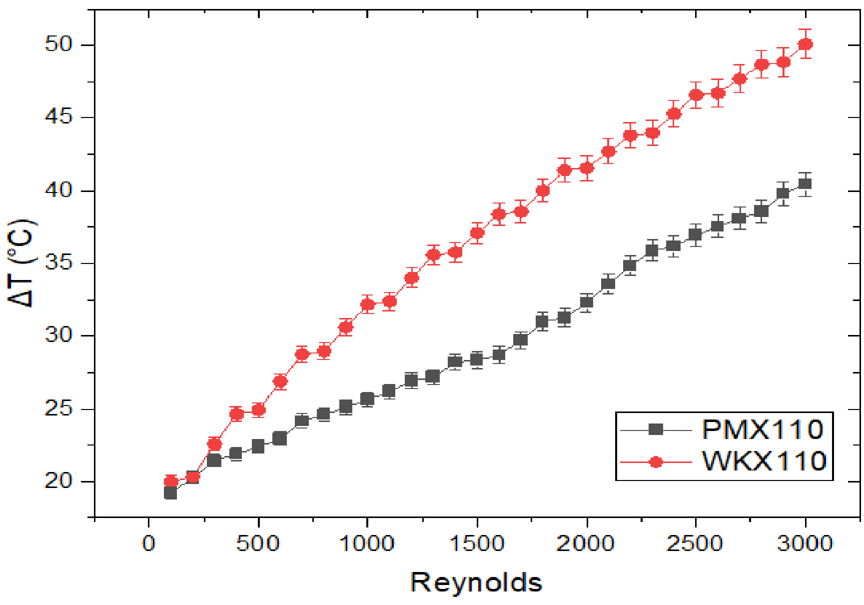

Figure 7. Enhancement Criterion for the Reynold's number and heat transfer

Conclusion

The research focused on the design of fire tube STHE to overcome sagging and warping issues, as well as to achieve heat-exchange technology of temperature and pressure of high magnitude in a steam production environment. Tube-shaped heat-exchanger was chosen due to its reliability in harsh operation environments, such as minimal pressure drop on cold sides. The overall size of the heat-exchanger was established based on criterion of tube-to-tubesheet, and the findings were compared to experimental heat-exchanger performance data. The thermal and flow parameters of the heat-exchanger were simulated using ANSYS fluent commercial CFD software. The distributions of temperature, pressure, velocity, as well as coefficients of heat transfer of the heat-exchanger were studied. The numerical PMX110 and WKX110 findings were compared to experimental data and found to be in good agreement. In terms of modelling, an acceptable approximation of the overall performance of the heat-exchanger was accomplished by taking into account the main assumptions of generalization, model, geometrical meshing, and baffles design, as the results obtained with this model have a satisfactory level of accurateness comparing with operation dimensions. The primary changes seen in the outflow were anticipated due to the overall hot flue mechanisms in conjunction with the Finite Rate/Eddy-Dissipation technique. Taking into account the temperature increases achieved by the multiple baffles in the new design, WKX110 is more acceptable in solving the primary problems encountered by PMX110 in terms of low temperature and pressure drop with high energy dissipation; however, PMX110 maintained high velocity output. Because of the position of the fluids in the heat-exchanger, the results produced with this model outperform those in literature. The employment of numerous operational functions in a consecutive optimization strategy achieves this increase in outcomes. As a result, the model may be employed to investigate design and analysis of control systems, as well as to aid in the formulation of operating techniques in various situations. The information can also be used to evaluate operational factors that are not quantifiable in engineering assessment.

References

Bougriou, C., & Baadache, K. (2010). Shell-and-double concentric-tube heat exchangers. *Heat and mass transfer*, *46*, 315-322.

Brackbill, J. U., Kothe, D. B., & Zemach, C. (1992). A continuum method for modeling surface tension. *Journal of computational physics*, *100*(2), 335-354.

Costa, A. L., & Queiroz, E. M. (2008). Design optimization of shell-and-tube heat exchangers. *Applied Thermal Engineering*, *28*(14-15), 1798-1805.

Dubey, V. V. P., Verma, R. R., Verma, P. S., & Srivastava, A. (2014). Performance analysis of shell & tube type heat exchanger under the effect of varied operating conditions. *IOSR Journal of Mechanical and Civil Engineering (IOSR-JMCE)*, *11*(3), 08-17.

Fadhl, B., Wrobel, L. C., & Jouhara, H. (2015). CFD modelling of a two-phase closed thermosyphon charged with R134a and R404a. *Applied Thermal Engineering*, *78*, 482-490.

García-Valladares, O. (2004). Numerical simulation of triple concentric-tube heat exchangers. *International journal of thermal sciences*, *43*(10), 979-991.

Gomaa, A., Halim, M., & Elsaid, A. M. (2016). Experimental and numerical investigations of a triple concentric-tube heat exchanger. *Applied Thermal Engineering*, *99*, 1303-1315.

Huzayyin, A., Nada, S., & Elattar, H. (2007). Air-side performance of a wavy-finned-tube direct expansion cooling and dehumidifying air coil. *International journal of Réfrigération*, *30*(2), 230-244.

Jouhara, H., Fadhl, B., & Wrobel, L. C. (2016). Three-dimensional CFD simulation of geyser boiling in a two-phase closed thermosyphon. *International Journal of Hydrogen Energy*, *41*(37), 16463-16476.

Khayal, O. M. E. S. (2018). Fundamentals of Heat Exchangers. *International Journal of Research in Computer Applications and Robotics*, *6*, 1-11.

Kuzmin, D., & Hämäläinen, J. (2014). *Methods for Computational Fluid Dynamics: A Practical Guide*. SIAM.

Liang, S., Liu, M., Wong, T., & Nathan, G. (1999). Analytical study of evaporator coil in humid environment. *Applied Thermal Engineering*, *19*(11), 1129-1145.

Nsofor, E. C., Celik, S., & Wang, X. (2007). Experimental study on the heat transfer at the heat exchanger of the thermoacoustic refrigerating system. *Applied Thermal Engineering*, *27*(14-15), 2435-2442.

Pandita, M. K., Gupta, A. K., & Lahadotiya, K. K. (2023). CFD analysis of a single shell and single tube heat exchanger and determining the effect of baffle angle on heat transfer. *International journal of engineering sciences & research technology*.

Raj, K. T. R., & Ganne, S. (2012). Shell side numerical analysis of a shell and tube heat exchanger considering the effects of baffle inclination angle on fluid flow using CFD. *Thermal Science*, *16*(4), 1165-1174.

Samal, A. K. (2013). *Shell and tube heat exchanger design using CFD tools*.